

A Power-Efficient Neural Tissue Stimulator With Energy Recovery

Shawn K. Kelly, *Member, IEEE*, and John L. Wyatt, Jr., *Senior Member, IEEE*

Abstract—This paper presents a power-efficient neural stimulator integrated circuit, designed to take advantage of our understanding of iridium-oxide electrode impedance. It efficiently creates a programmable set of voltage supplies directly from a secondary power telemetry coil, then switches the target electrode sequentially through the voltage steps. This sequence of voltages mimics the voltage of the electrode under the constant current drive, resulting in approximately constant current without the voltage drop of the more commonly used linear current source. This method sacrifices some precision, but drastically reduces the series losses seen in traditional current sources and attains power savings of 53%–66% compared to these designs. The proof-of-concept circuit consumes 125 μW per electrode and was fabricated in a 1.5- μm CMOS process, in a die area of 4.76 mm^2 .

Index Terms—Biomedical engineering, bioelectric potentials, biomedical electrodes, integrated-circuit (IC) design, iridium, neuromuscular stimulation, retinal prosthesis, telemetry.

I. INTRODUCTION

NEURAL AND muscular stimulators, used in cochlear implants, cardiac pacemakers, and other medical devices [1]–[5] deliver electrical current to tissue, typically from a current source of traditional design. These traditional sources use a significant voltage drop across a transistor to maintain constant current, and draw current from large dc voltage supplies, consuming power (for the stimulation parameters used in this work) of 373 μW per electrode for a typical design, or 271 μW per electrode for a very aggressive design (more aggressive than those found in published work). Our stimulator with programmable voltage steps uses 125 μW per electrode, 53% less than an aggressive design, and 66% less than a design typically in use [6]. The difference in these power numbers, 146–248 μW , is waste due to the voltage supported by the current source transistors. This waste power, of course, is released as heat to the surrounding tissue [7], threatening tissue damage. The retina, for which this stimulator was designed,

is particularly sensitive to temperature-induced damage, including damage to the retinal ganglion cells [8], and present estimates predict that the number of electrodes in a retinal implant will be in the high hundreds or low thousands. In addition to increasing heat dissipation at the stimulator, higher power consumption also exposes the body to larger magnetic fields, due to the demand for higher power transmission from the external battery power supply. The IEEE and ANSI have a joint standard which recommends an occupational limit for magnetic-field exposure that decreases as frequency increases between 100 kHz and 100 MHz [9]. This system and others already exceed this recommended field-frequency product of 16.3 MHz·A/m [10], [11], and greater power consumption in the stimulating electronics necessarily means a greater need for power transmitted via magnetic fields. Of the 125 μW consumed in our stimulator system, 49 μW is consumed in the electrodes, calculated directly from the product of electrode current and voltage. The difference in these power numbers, 76 μW , is power wasted in the switches and in power-management inefficiencies. Nonetheless, these losses are small compared to the power savings over traditional current source designs.

Several factors that determine power consumption may be out of the control of the designer (e.g., threshold for perception or function, electrode size, or material). But several steps may still be taken to reduce the consumed power for a stimulator, and the stimulator presented here uses a novel architecture to drastically reduce the wasted power. This architecture implementation is similar in some ways to the adiabatic circuits used to reduce power in digital design [12], [13]. Our scheme can also be combined with algorithmic strategies to reduce power [14], [15].

This architecture minimizes the power lost in driving the electrodes in our wireless-implanted stimulator. The electrode drive power dominates the communication and control power in this system, as in any system with a large number of electrodes. This paper uses a simple and conservative accounting method for total implant power: the system power consumption figures include all of the power dissipated in and delivered by the implanted secondary power telemetry coil.

A. Overview

The low-power stimulation method depends on careful analysis of power consumption in a basic linear model of the electrode, which is developed in Section II. Section III derives the power cost for a traditional current source drive and explains the origin of the inefficiency. Section IV introduces a more efficient strategy for driving the same total charge through an electrode over the same time interval, and Section V gives the basic architecture and current and voltage waveforms to implement

Manuscript received August 25, 2009; revised April 28, 2010; accepted August 22, 2010. Date of current version January 26, 2011. This work was supported by a fellowship from the Catalyst Foundation; MOSIS provided fabrication. This paper was recommended by Associated Editor G. Cauwenberghs.

S. K. Kelly is with the Center for Innovative Visual Rehabilitation, Boston, MA 02130 USA. He is also with the Research Laboratory of Electronics, Massachusetts Institute of Technology, Cambridge, MA 02139 USA (e-mail: skkelly@alum.mit.edu).

J. L. Wyatt, Jr. is with the Research Laboratory of Electronics and Department of Electrical Engineering and Computer Science, Massachusetts Institute of Technology, Cambridge, MA 02139 USA. (e-mail: jlw@mit.edu).

Color versions of one or more of the figures in this paper are available online at <http://ieeexplore.ieee.org>.

Digital Object Identifier 10.1109/TBCAS.2010.2076384

this strategy. Section VI develops the architecture in more detail and gives the transistor-level circuit designs for all the novel elements in the system. Section VII gives results for an experimental chip, and Section VIII lists the conclusions.

II. ELECTRODE-TISSUE INTERFACE—CIRCUIT MODEL AND POWER CONSUMPTION

For the experiments in this paper, we used polyimide thin-film arrays, with activated iridium-oxide film (AIROF) electrodes. AIROF electrodes have a higher published safe charge density limit than other stimulating materials, roughly 10–30 times that of platinum, depending on the stimulation parameters [16]. The AIROF electrodes used in this paper were 400 μm in diameter, and were the same material and dimension as those used in several acute human stimulation experiments by our group [17], [18]. For the stimulus currents and charges of interest, these electrodes may be modeled as a series resistor and capacitor, as shown in Fig. 1(a). The capacitor represents the charge boundary layer at the metal-fluid interface and oxidation state change of iridium, whereas the resistor represents the fluid resistance and the access resistance of the lattice structure of the iridium-oxide film. More complex electrode models exist, generally with some form of conductance in parallel with the metal-fluid interface capacitor. Some models include a constant-phase element [19]. For the purposes of this proof-of-concept system, and for the pulsewidths used in this design, the simple model in Fig. 1(a) is sufficient, as will be shown in our bench-top studies. The electrodes are typically driven by a charge-balanced, biphasic pair of constant current pulses, shown in Fig. 1(b). The resulting voltage across the electrode resistance and capacitance is the step-ramp waveform that is shown. The parallel resistance and constant-phase element, not shown in Fig. 1(a), will curve the ramping portion of the waveform in Fig. 1(b) slightly, with the former element reducing the slope later in the ramp portion, especially over very long pulses, and the latter element softening the sharp corner at the step-ramp transition. Since the circuits described here merely approximate the electrode voltage waveform, these two elements can be omitted without major consequences.

We assume, based on prior human experiments [17], [18], that the required threshold charge is fixed over some range of stimulus pulse durations (0.25–8 ms per phase), and that the total integrated charge matters more than the specific stimulation waveform. These assumptions are based on our epiretinal human experiments, but they may not hold for subretinal stimulation. We also assume that the electrode resistance is fixed by electrode geometry, which, in turn, is constrained by biology and charge density limits. The capacitance can vary based on its electrochemical preparation. Based on previous measurements of electrodes we used in human trials, we planned for an electrode resistance of approximately 1.1 k Ω ; the capacitance, 1 μF ; the delivered charge, 1 μC . However, the electrodes we used for these experiments had impedances far from the expected value: 2.3 k Ω and 0.49 μF . Because of this discrepancy, two electrodes were used in parallel to test this proof-of-concept circuit, giving test values of 1.15 k Ω and 0.98 μF for our system. The charge delivered by our prototype system to this two-electrode set during a 5-ms pulse was 0.678 μC , for an average current

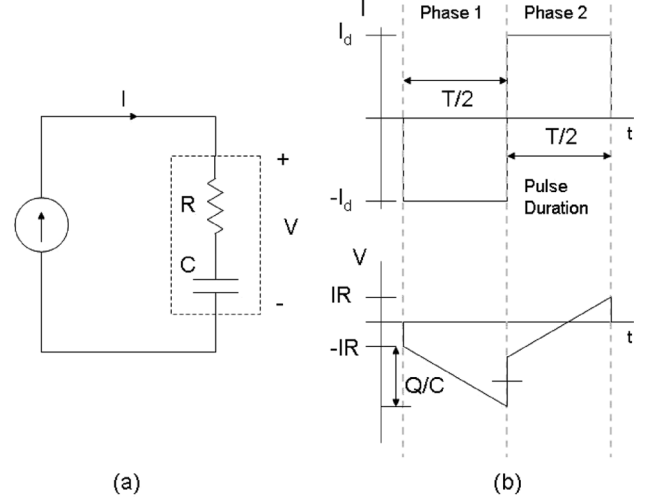


Fig. 1. Electrode model and stimulation waveforms. (a) Current source drives the series resistance and capacitance of the stimulating electrodes. (b) Charge-balanced biphasic current waveform is typically used, giving the voltage waveform shown.

of 136 μA . The reverse average current was then applied for an additional 5 ms to balance the charge, for a total stimulus of 10 ms, at a repetition rate of 100 Hz.

Power consumption within the electrode occurs in the resistive portion. Therefore, the theoretical minimum power required to drive the electrode with current I , or more appropriately, to drive the electrode to charge Q in time $T/2$ (one phase of the biphasic waveform), is simply

$$P = I^2 R = \frac{4Q^2 R}{T^2}. \quad (1)$$

This is the power consumed within the electrodes. The first lesson to be learned from (1) is that if Q and R are fixed, power depends only on pulse duration, and longer durations of stimulation at lower currents reduce the power consumed by the electrodes. The architecture presented here works well at longer duration pulses, but the reduction in power for longer pulses applies to any stimulation architecture as long as the supply voltages are correspondingly reduced. This duration is subject to biological constraints, engineering constraints, and the constraint that the constant threshold charge assumption remains valid. Furthermore, different stimulation current pulse durations may generate qualitatively different responses in neural tissue [20], [21].

The second lesson that may be learned from (1) is that the power consumed within the electrodes is quite low. For charge $Q = 0.678 \mu\text{C}$ delivered in pulsewidth $T/2 = 5 \text{ ms}$ (average current $I = 136 \mu\text{A}$) through resistance $R = 1.15 \text{ k}\Omega$, the power consumed within the electrodes is 21.2 μW per electrode. As we will show in the next section, this is far lower than the power consumed by typical stimulators.

III. TRADITIONAL CURRENT SOURCE STIMULATOR DESIGNS

A typical current source works by connecting the load to a voltage supply through a transistor, which acts as a large variable series resistor to limit the current. The power consumption

depends only on the current and the voltage supply, and is otherwise independent of current source design. Delivering the same $136 \mu\text{A}$ used before from $\pm 2.5\text{-V}$ supplies or more, as is often done [5], results in $339 \mu\text{W}$ or more of the total power consumption per current-source/electrode pair during stimulation. Since our design incorporates the power converter circuitry, we assume that a 0.25-V Schottky diode is used to generate the power supply, raising the consumed power to $373 \mu\text{W}$ per electrode. Since our system uses $\pm 1.75\text{ V}$ supplies, we will compare to a current source system with the same supplies. With the added Schottky diode, this system would consume $271 \mu\text{W}$ per electrode. This is a fair comparison, given our system voltage supplies, but a neural stimulator with $\pm 1.75\text{ V}$ supplies would be considered to be a very aggressive, low-power design, and we have not found a published example with supplies this low.

The power consumed per electrode by a current source stimulator is far greater than the $21.2 \mu\text{W}$ per electrode calculated in Section II. This smaller power value is consumed within the electrode, in the unavoidable fluid and lead resistance. It is assumed here, but not tested, that any dielectric losses in the electrode capacitance are negligible compared to the losses in the resistance. The remainder of the current source power, $250 \mu\text{W}$ for the aggressive design or $352 \mu\text{W}$ for the more typical design, is consumed in the current source transistors or power circuitry. These energy transfer efficiencies of $\sim 8\%$ or $\sim 6\%$ show that the vast majority of expended power is consumed somewhere other than the electrodes and stimulated tissue.

Despite the energy inefficiency, there are nonetheless a number of benefits to this traditional current source design. The higher supply voltage leaves room for cascode stages and more linear current sources. It also allows for shorter duration pulses of higher current, which may be desired in some cases. In addition, the higher voltage supply allows for substantial variation in the load impedance, as might occur with tissue growth over the electrodes. These benefits permit the current source to maintain constant current during a variety of stimulation pulses, but the quality of the constant current pulse may be less valuable in some applications than a reduction in power consumption. In the following section, we will explore methods of trading off current source performance for power reduction.

IV. REDUCING SOURCES OF LOSS

Fig. 2 shows a different view of the electrode power and wasted power in a traditional current source. Fig. 2(a) shows the product of the electrode current and voltage waveforms from Fig. 1(b). This product is the power delivered into the electrode during stimulation. The shaded area in Fig. 2(a) is the energy stored in the electrode capacitance. Since this capacitive energy is returned in the second phase, the average of the whole power waveform is I^2R , as shown. Note that at the beginning of the second phase, the power delivered to the electrode is negative. During this time, the electrode in this example is sourcing power from its capacitance.

In Fig. 2(b), the same waveform is shown, but with the power supplied by the current source shown as a straight line across the top. The shaded area represents the wasted power burned in the current source transistors.

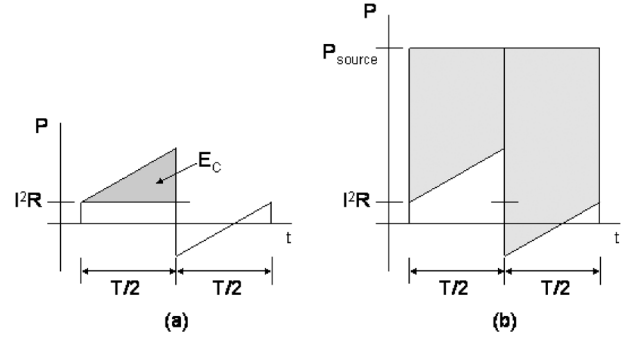


Fig. 2. Electrode power consumption and current source power. (a) Power delivered to the electrode, with the capacitive stored energy shown in the shaded region. (b) Power supplied by a traditional current source, with the wasted power shown in the shaded region.

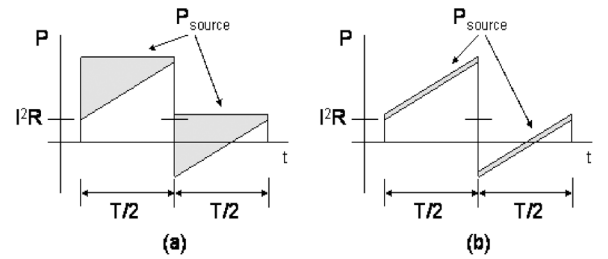


Fig. 3. Current source power consumption. (a) Power supplied by the current source with reduced voltage supplies, with the wasted power shaded. (b) Power supplied by a nearly ideal source with nearly zero voltage drop above the electrode voltage.

A. Reducing Excess Voltage Drops

The wasted power in Fig. 2(b) can be reduced by simply lowering the voltage supplies from which the current is drawn, resulting in the power shown in Fig. 3(a). With lower currents delivered over longer pulse widths, as recommended in Section II, this supply voltage can be made quite low. The complication is that the voltage compliance requirements vary with electrode impedance and drive current, so that the voltage supply must be variable. In addition, if the voltage compliance is reduced too far, the voltage supplies may not support the analog and digital control and communication circuitry required for the implant. Thus, this method of power reduction may require independent voltage supplies. The constant, higher voltage control circuitry supply may be generated simply from the receiver coil with diodes. The variable, lower voltage supply must be generated by some sort of efficient active rectification or power conversion. Work has been done on efficient dc-dc converters and active synchronous rectifiers [22], [23], but most of these circuits are designed for high-power applications. Our solution needs to use very little standby power and no additional inductors, due to space constraints.

B. Delivering Current With Minimum Power and With Energy Recovery

To eliminate the remaining shaded triangles in Fig. 3(a), a current source could be conceived whose voltage tracks the back voltage on the electrode. This current source would have virtually no wasted power dissipation, as shown in Fig. 3(b). As before, note that in the beginning of the second phase in Fig.

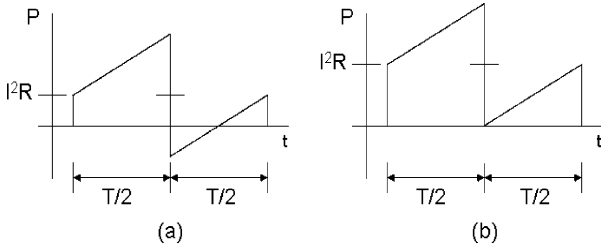


Fig. 4. Sample power waveforms. (a) Power is recovered in the first half of the second phase, but no net energy is recovered. (b) No power is recovered during the second phase.

3(b), the electrode capacitance is returning power to the current source. During this time, the stimulator is recovering power from the electrode, and during the second phase shown in Fig. 3(b), the stimulator recovers net energy from the electrode.

This power and energy recovery does not always take place, and depends on the ratio of the electrode RC time constant to the pulse duration. Fig. 4(a) shows an example power waveform with power recovery at the beginning of the second phase, but zero net second phase energy recovery. This occurs when the maximum voltage across the capacitor is twice the voltage across the resistor, or

$$\begin{aligned} \frac{IT}{2C} &= 2IR \\ RC &= \frac{T}{4}. \end{aligned} \quad (2)$$

Fig. 4(b) shows a case in which no power is ever recovered from the electrode. This occurs when the maximum capacitive voltage and the resistive voltage are equal, or

$$RC = \frac{T}{2}. \quad (3)$$

C. Approximate Voltage Waveform

The current source behavior in which the voltage supply follows the ramping electrode voltage waveform as in Fig. 3(b) may be approximated by a series of voltage steps. Fig. 5(a) repeats the electrode current and voltage waveforms for convenience, and Fig. 5(b) shows the stepped voltage waveform and resulting current.

A stimulator with this stepped voltage waveform will deliver current with some ripple, but that current integrates to the same stimulus charge in the electrode capacitance. While this stimulation method can reduce waste power consumption, it requires the series of supply voltages to be generated efficiently. This is achieved by the stimulator architecture as will be explored below.

V. VOLTAGE STIMULATION ARCHITECTURE WITH ENERGY RECOVERY

The voltage steps for stimulation may be implemented with a bank of power-supply capacitors. Fig. 5(b) shows four voltage steps per stimulation phase, the number used in our system. It is shown theoretically in [11, App.] that using five, four, and three voltage steps consumes 9%, 15%, and 32%, respectively, more than the minimum required I^2R power. A four-step system was

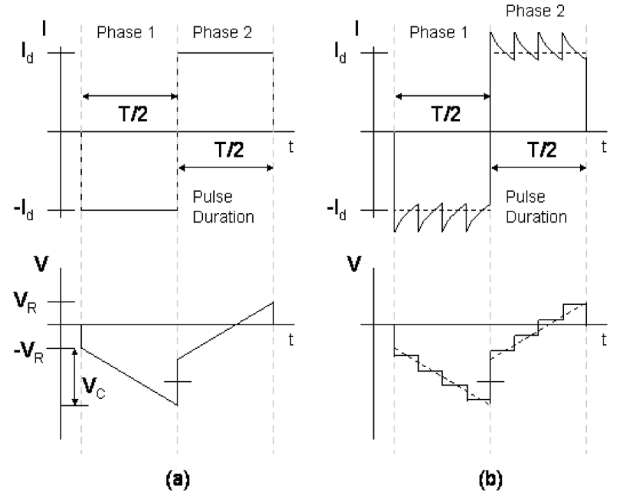


Fig. 5. (a) Repetition of electrode current and voltage waveforms. (b) Approximate waveforms using a voltage step stimulator.

chosen as a reasonable compromise and to simplify the digital state machine design. It is important to point out that this step voltage system is only created once, globally, and that the only circuits repeated for each electrode are the switches to connect to the steps.

Note that the four-step system as shown in Fig. 5(b) uses eight different voltages in the two phases. This can be simplified in three ways. First, any voltage levels in the positive and negative phases that are near each other can be combined to use only one capacitor. Second, any voltage level that is near ground may be replaced by ground, eliminating a capacitor. Third, the number of first- and second-phase voltage levels that are near each other may be increased by making the capacitive ramp voltages of the two phases overlap more. This is done by reducing the IR voltage relative to the Q/C voltage. Since R , C , and Q are fixed, the current should be reduced and the phase duration increased. Using these methods, we were able to simplify the eight voltage sources down to five. An additional consideration which simplifies the power converter design in the next section is that, for cathodic-first stimulation, AIROF electrodes work best with a slight anodic bias [16]. This dc voltage may cause some concern, but at a modest anodic bias, the leakage current is low enough to be supported by noninjurious reactions with the fluid buffer. This biasing is commonly done with iridium-oxide electrodes, and is considered to be a safe practice [24], though it has not been used in human trials. This anodic offset eases the requirements on the power converter by balancing the demands between the positive and negative phases of the power secondary coil voltage. In other words, instead of creating four negative supplies and one positive supply, the power converter creates three negative and two positive supplies, as shown in Fig. 6(a) and (b).

The anodic bias is equal to one voltage step, so the electrodes are biased to voltage V_{cp1} . As shown in Fig. 6(b), the electrode is switched from V_{cp1} first to V_{mid} (the electrode current return), then to V_{cn1} , V_{cn2} , and V_{cn3} to generate the negative current, then to V_{cn1} , V_{mid} , V_{cp1} , and V_{cp2} to generate the positive current. Electrodes are drawn back to V_{cp1} between stim-

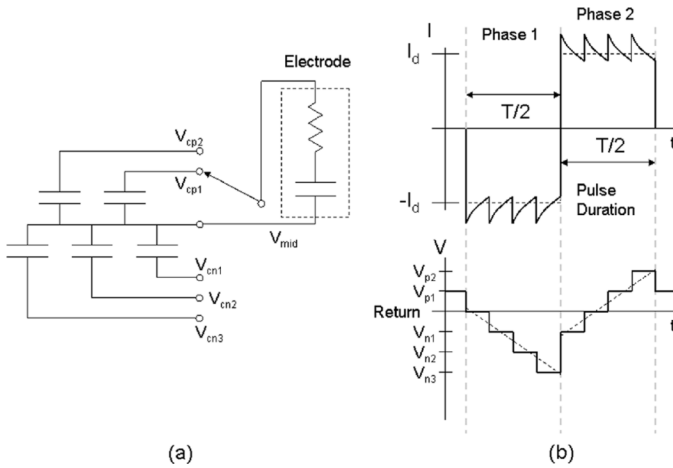


Fig. 6. (a) Architecture of a four-step, five-capacitor voltage step stimulator with one-step anodic bias. (b) Approximate current and voltage waveforms.

ulus pulses by a very weak (200 nA) current source. Notice that voltages V_{cn1} and V_{mid} are visited in the negative and positive directions. While V_{mid} is a direct connection to the circuit midpoint created by the dual half-wave rectifiers, voltage V_{cn1} is a supply capacitor, which is discharged slightly when supplying negative current to the electrode, and recharged slightly when supplying positive current. Thus, the stimulation system is recovering energy from the electrodes to this supply capacitor during the second phase of the stimulation.

A. Bench Experiments

To test the concepts presented before, an electrode in physiological saline was driven by an arbitrary voltage waveform generator first in the optimal step-ramp pattern described in Section IV-B and Fig. 3(b), then in the stepped pattern described in this section and in Fig. 6. A simple current sense amplifier served as the return path, sensing current through the electrode. The results of these experiments are shown in Fig. 7. Fig. 7(a) shows the step-ramp voltage waveform and resulting current. Note the consistency in the current plot which shows overlaid data from five different measurements. Note also that the current waveform is not square. The initial peak in the current is due to the nonidealities of the electrode impedance. Fig. 7(b) shows the four-step voltage system described earlier in this section and its resulting current waveform.

VI. SINGLE-COIL MULTIVOLTAGE POWER SUPPLY USING A CONTROLLED SYNCHRONOUS RECTIFIER

The capacitive voltage supplies described before are created from a single ac voltage on a secondary coil by means of a controlled synchronous rectifier. This rectification step must be done efficiently for this stimulator to save any power. In addition, because of the small power budget (~ 10 mW) and size restrictions for the retinal implant, dc/dc switching power converters were not seriously considered. The chip power supply for control circuitry is generated by two simple half-wave rectifiers, using Schottky diodes.

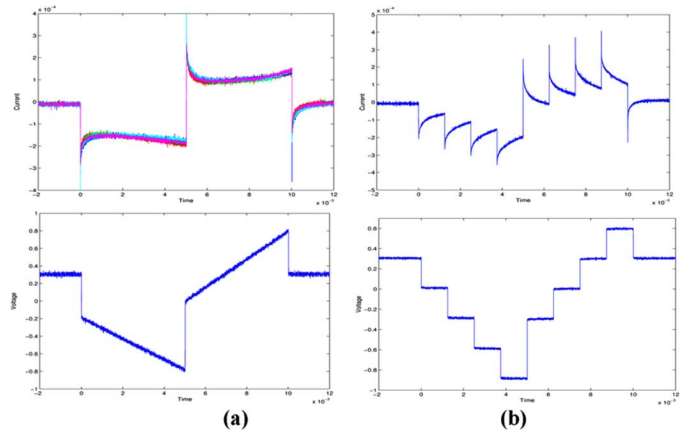


Fig. 7. Bench electrode drive test results with an arbitrary voltage waveform generator (bottom graphs) and the resulting current through the electrodes (top graphs). Part (a) shows an ideal step-ramp voltage drive, while (b) shows a four-step stimulating voltage drive.

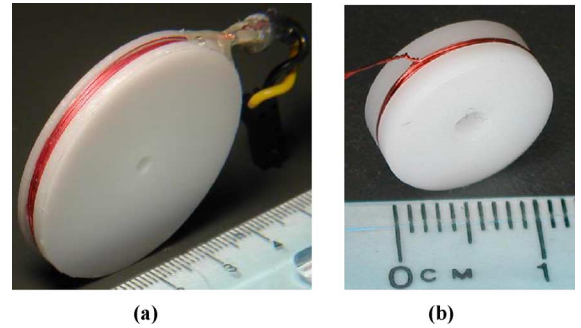


Fig. 8. (a) Primary and (b) secondary power telemetry coils used in this paper.

A. Inductive Power Transmission

Power is delivered to the implant chip via an inductive link at 125 kHz. We hand-wound primary and secondary coils on plastic forms. The primary coil, shown in Fig. 8(a), consists of 45 turns of 30 AWG wire with a mean diameter of 37 mm and inductance of $153 \mu\text{H}$. The secondary coil, shown in Fig. 8(b), consists of 60 turns of 36 AWG wire with a mean diameter of 11 mm and an inductance of $58 \mu\text{H}$. The primary is driven by a class E power amplifier, and the secondary is held 15 mm from the primary in a nonconductive plastic test jig. The primary drive current is set so that the voltage at the secondary coil yields ± 2.5 -V power supplies after the dual half-wave Schottky rectifiers.

B. Synchronous Rectifier Chip Architecture

The controlled synchronous rectifier forms the core of this design, and its architecture is shown in Fig. 9. On the left, a V_T -based reference is used, and is buffered for the chip's pbias and nbias. The rectifier reference voltages are then derived in the box labeled Vref, which feeds a constant current through a string of on-chip resistors. These reference voltages determine the voltage to which the supply capacitors will be charged. They are buffered and sent to the column of clocked comparators near the middle of Fig. 9, where the supply capacitor voltages are compared to the references on every cycle. Below the clocked comparators, the clock generation circuitry is shown. A clock is extracted from the 125-kHz coil voltage, labeled ac throughout

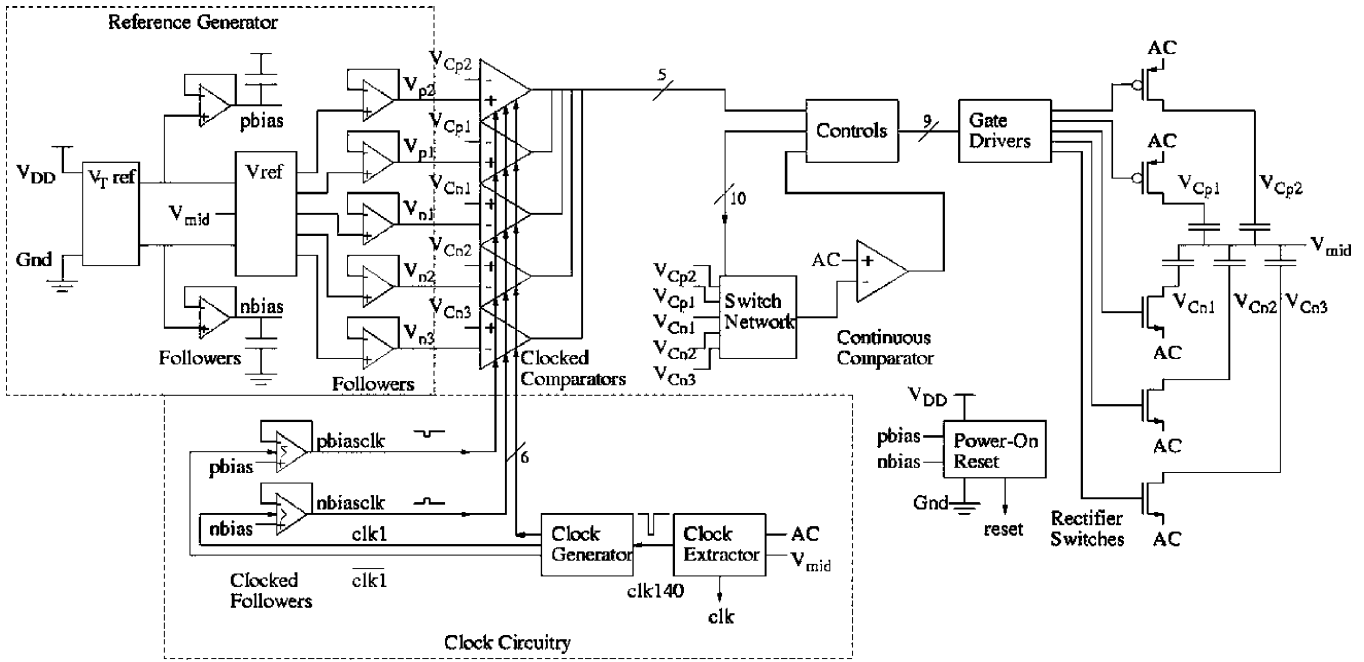


Fig. 9. Block diagram architecture of the synchronous rectifier chip. The capacitor voltages are compared to the generated reference voltages (upper left). Any capacitor needing charge is connected to the ac supply when the ac voltage exceeds that capacitor’s voltage (center, upper right).

the figure, and turned into a sequence of clock edges for the comparators. The comparator outputs feed into the control circuitry, which, in part, determines which supply capacitor will be monitored by the continuous comparator. This comparator turns on the appropriate rectifier switch, via the control circuitry, when the ac voltage exceeds the monitored capacitor voltage. Finally, a power-on reset circuit ensures that all circuits initialize to a known state.

C. Rectifier Reference Voltages

The controlled synchronous rectifier works by turning on a rectifier switch between the secondary coil and the supply capacitors, charging the capacitor up to a specified reference voltage. The reference voltages are created by driving dc current through a string of on-chip polysilicon resistors. The current is determined by a V_T -based reference and three off-chip selector switches. This reference circuit is shown in Fig. 10. We typically set the voltage steps to between 0.12 and 0.25 V, but the full range of the supplies is from 0.07 to 0.33 V. This voltage selectability allows the stimulator to account for a wide range of electrode impedances or tissue stimulation thresholds. In a tissue stimulator for human use, more flexibility may be required.

D. Clocked Comparators

The supply capacitor voltages were compared to the buffered reference voltages in a very sensitive clocked comparator, shown in Fig. 11. The core of this circuit is the cross-coupled inverter pair formed by MN1, MP1, MN2, and MP2. The circuit works by allowing the inputs to take control of the weakened inverter pair, after which the inverter pair is powered to latch the result. Specifically, each inverter has two connections to each power supply: 1) a constant weak one, through transistors

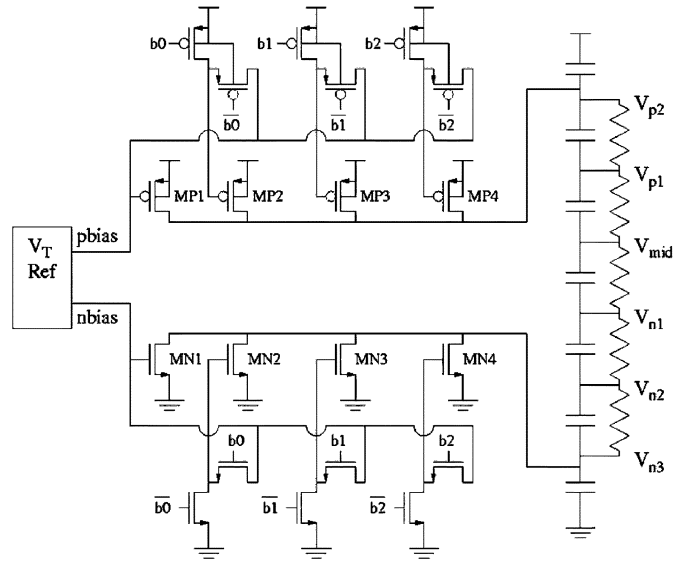


Fig. 10. Reference voltage generator. A V_T -based reference generates selectable currents which run through a string of polysilicon resistors to set up voltage step references.

MP3, MP4, MN3, and MN4, connected to pbias and nbias, and 2) a clocked strong one, through transistors MP5, MP6, MN5, and MN6, connected to pCLK and nCLK. In a comparison, the cross-coupled inverters are first weakened (pCLK and nCLK turned off). Next, the dual differential pairs made up of MN7 and MN8, and MP7 and MP8 are powered (pbiasCLK and nbiasCLK turned on), the passgates from the differential pairs to the cross-coupled inverters are enabled (CLK1 on), and the passgates to the output latch are disabled (CLK2 off). The differential pairs control the inverter pair based on the capacitor and reference voltages, and then the clocks are reset in the

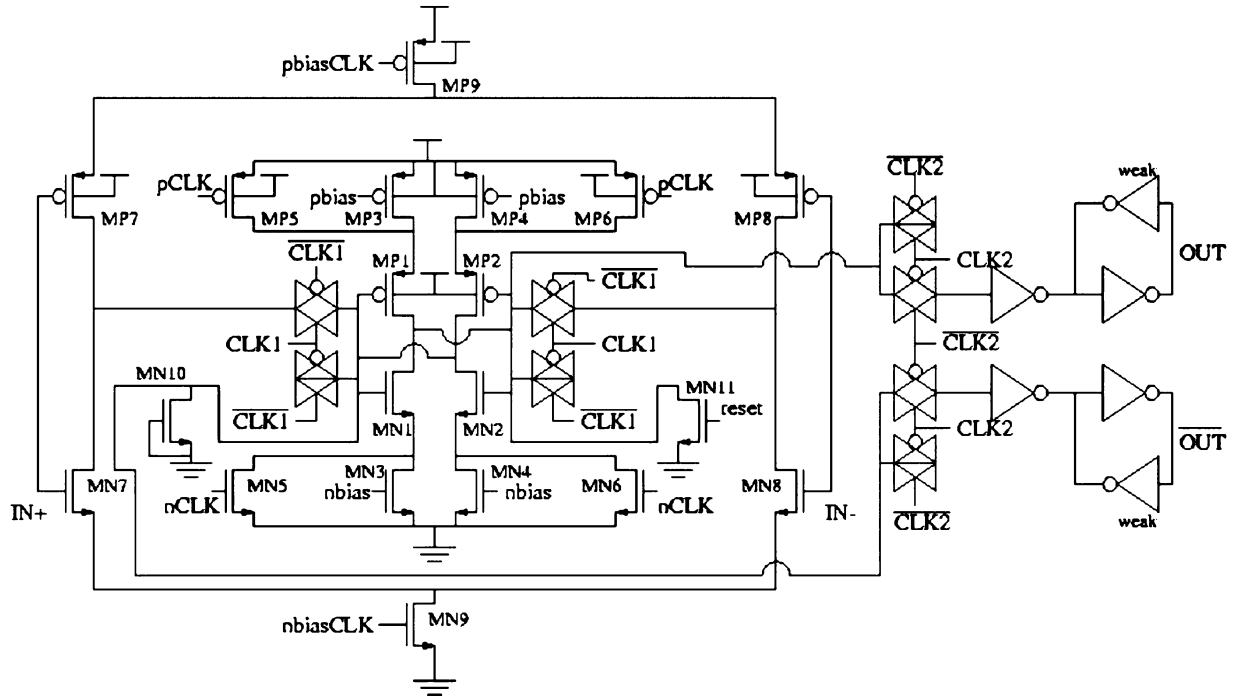


Fig. 11. Clocked comparator. The cross-coupled inverter pair formed by MP1, MP2, MN1, and MN2 latches the difference between inputs IN+ and IN-. The inverter pair is weakened during sampling by turning off pCLK and nCLK.

same sequence. The cross-coupled pair first engages to latch the comparison (pCLK, nCLK), then the differential pairs turn off, the input passgates disable, and the output passgates enable (pbiasCLK, nbiasCLK, CLK1, CLK2).

E. Continuous Comparator

The timing for turning on the rectifier switches to charge the supply capacitors is determined by a continuous comparator, which monitors the ac coil voltage and a selected capacitor. This is shown in the middle of the diagram in Fig. 9. This comparator needs to be fast enough to follow the rising edge of our 125-kHz power coil and turn on the rectifier switch with negligible delay, yet consume little power. This is accomplished by using a predictive front end, slightly modified from that described by MeVay and Sarpeshkar in [25]. This comparator architecture, shown in Fig. 12, uses a self-biased Bazes very wide common-mode range differential amplifier (VCDA) [26] for rail-to-rail comparator operation at only $54 \mu\text{W}$, but adds the predictive front end to shift the dc comparison voltage based on the slope of the ac voltage. The capacitor on the left of the figure injects into the mirrors a current proportional to the slope of the ac voltage. This current is mirrored via either MP1/MP2 or MN1/MN2 into the resistor connected to the dc voltage, and the modified voltage is used for the comparison. For example, if the ac voltage is rising, current is injected into MN1, and MN2 draws current out of the resistor. This lowers the compared voltage, causing the comparator to begin to change state earlier. If the predictive time shift can be matched to the comparator delay, a low-power comparator can be made to have a very small delay. The other mirrors in Fig. 12, with transistors numbered 3 through 5, are added in this paper to give first-order cancellation of the resistive current at the dc

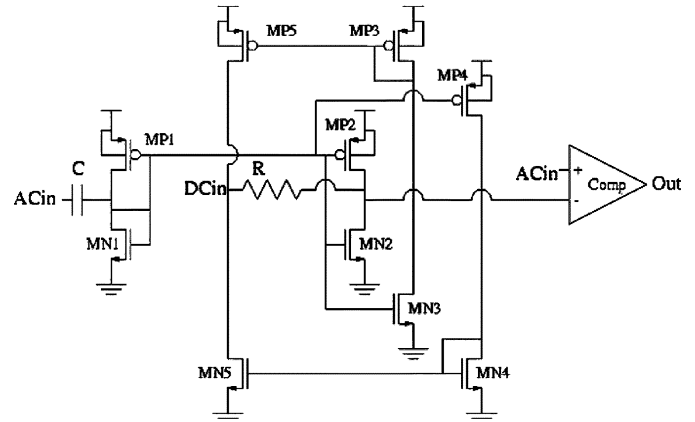


Fig. 12. Predictive comparator front end. The ac input injects current into the mirror, which is drawn through the resistor connected to the dc input. The ac voltage is compared to the dc voltage minus a component proportional to the slope of the ac. The mirrors created by MN3, MP3, MN4, MP4, MN5, and MP5 form a first-order current cancellation circuit.

voltage node. The predictive comparator used here in a synchronous rectifier role has a very low power-delay product in a low-power application where losses need to be eliminated. A faster traditional comparator would consume too much current, and a slower comparator would cause too much turn-on delay, increasing losses in the rectifier switches.

VII. RESULTS

This low-power stimulator chip, shown in Fig. 13, was fabricated in a $1.5 \mu\text{m}$ CMOS process and tested with a wireless inductive power supply and preprogrammed data. The system drove a set of 15 iridium-oxide electrodes in a buffered saline solution, with a separate return electrode that was much larger

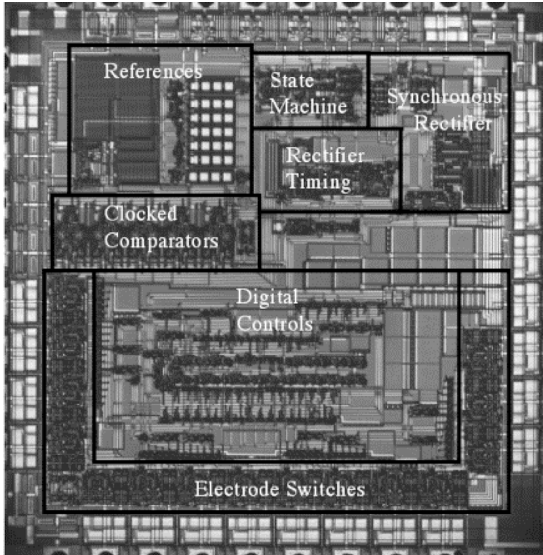


Fig. 13. Die photograph of the low-power stimulator chip.

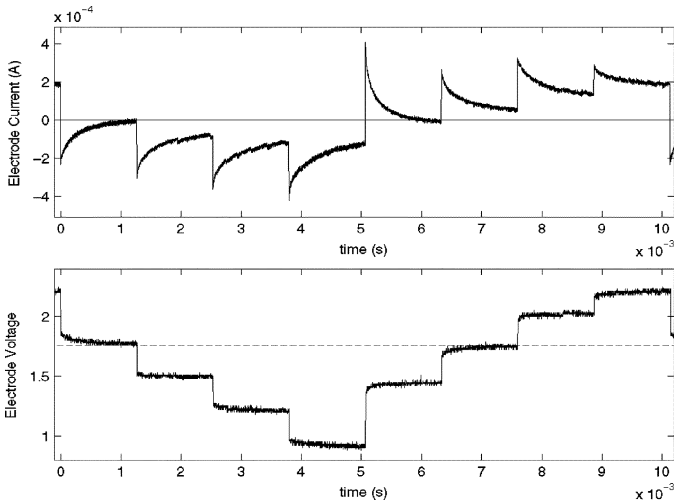


Fig. 14. Measured electrode current and voltage waveforms. Compare the current and voltage waveforms to those predicted in Fig. 6(b). Voltage waveforms here are with respect to the chip ground, not V_{mid} .

than the sum of the electrode areas. Electrode current was measured with a small series resistor and an instrumentation amplifier. The measured electrode current and voltage waveforms are shown in Fig. 14. Note the similarities between the predicted waveforms in Fig. 6(b), the measured waveforms in Fig. 7(b), and the measured waveforms in Fig. 14. The voltage waveform is very close to the desired waveform, while the current has slightly higher peaks than desired for optimal efficiency. The current in Fig. 14 integrates to $0.678 \mu\text{C}$ per phase, close to our measured human epi-retinal perceptual threshold of $0.8 \mu\text{C}$.

Power consumption for the entire system was calculated directly from the secondary coil voltage and current, measured by an instrumentation amplifier. This gave the total power consumed downstream from the coil. The I^2R dissipation of the coil was then added to that value. These values account for all of the power delivered to the secondary coil by the magnetic field. They were taken when driving no electrodes, and again when fully driving all 15 electrodes.

TABLE I
STIMULATOR SYSTEM POWER CONSUMPTION. POWER CONSUMED WHILE DRIVING 15 ELECTRODES, AND IN THE REST STATE WHILE DRIVING NO ELECTRODES

	15 Electrodes		No Electrodes	
	Mean	St.Dev.	Mean	St.Dev.
Coil Power	44.4 μW	14.1 μW	2.79 μW	0.11 μW
System Power	2.18 mW	0.691 mW	335 μW	20.1 μW
Total Power	2.22 mW	0.703 mW	338 μW	20.2 μW

The data in Table I show that the total power (including secondary coil losses) required to drive $0.678 \mu\text{C}$ into each of 15 electrodes at 100 Hz frame rate is 2.22 mW. Since the system consumes 338 μW of power with no electrodes driven, the cost of electrode stimulation, including all system inefficiencies, is 1.88 mW, or 125 μW per electrode. As stated before, a very aggressive traditional current source design using the same $\pm 1.75\text{-V}$ supplies created with an efficient 0.25-V Schottky diode rectifier, delivering the same charge in the same time, will use 271 μW per electrode. Our design represents a 53% power savings over such an extremely aggressive current source design. A more typical current source stimulator might use $\pm 2.5\text{-V}$ supplies using 373 μW per electrode, nearly three times the power consumption of our device. Most current source stimulators use much higher voltages than this in an attempt to improve current source output impedance and to hedge against future voltage compliance requirements that arise from impedance variations or stimulus threshold charge or current variations. The design presented here includes programmable voltage supply levels which can be designed with a broader range to give the minimum voltage required to drive the threshold charge into the electrodes, while reserving the capability to increase the voltage supplies at a later time to drive more charge or larger electrode impedances.

For reference, we know from (1) that the theoretical minimum power consumption within electrodes receiving this charge stimulation is 21.2 μW . We calculated the power delivered to the electrodes by our system from the product of the electrode voltage and current, and found 49 μW per electrode. Table II shows a comparison of all of these values. Let us consider the losses in this system, the difference between the theoretical 21.2 μW , measured 49 μW into the electrode, and measured 125 μW per electrode for the whole system. The 49- μW measured electrode power includes several inefficiencies, including the current peaking from using voltage steps as well as nonidealities in the electrode impedance. The 125- μW measurement is more obvious, as it includes losses in the rectifier switches and increased coil losses. To further reduce this power and increase efficiency, a voltage-based stimulation system could be designed which tracks the electrode voltage, as shown in the bench tests in Fig. 7(a).

VIII. CONCLUSION

The stimulation system presented here realizes power savings of 53% over an extremely aggressive traditional current source design and 66% or more over commonly used designs. It does this by using a voltage-based design, which has efficiency

TABLE II
COMPARISON OF POWER CONSUMED PER ELECTRODE

Theoretical	Minimum Possible Power	21.2 μW
This System	Measured Power Into Electrode	49 μW
This System	Net Power During Stimulation (Not Including Overhead)	125 μW
This System	Gross Power During Stimulation (Including Overhead)	148 μW
Aggressive Current Source System	Net Power During Stimulation (Not Including Overhead)	271 μW
Typical Current Source System	Net Power During Stimulation (Not Including Overhead)	373 μW

benefits over a current source design, but is generally avoided in neural and other tissue stimulators. This efficiency requires tradeoffs, resulting in decreased current precision and increased complexity of the power management system. A practical implementation of this system will require careful control of the step voltages and should include the ability to control the steps via telemetered data or by a current-feedback system on-chip. In a medical application, the architecture described here would require additional safeguards to measure and limit total charge delivered, but we believe that these safeguards can easily be added and that the power savings of this design justify the increased complexity.

A number of improvements can be made to a future design. First, a stepped voltage system such as that described here could use simple current sources instead of switches to connect the electrodes to the steps. This would limit the peak current to the electrodes and keep it closer to the constant-current waveform. In addition, as retinal prostheses implement more and more stimulating electrodes, the size of each electrode will likely decrease, with each electrode targeting a smaller number of retinal ganglion cells, and greater charge-delivery precision will be required. The simple current sources can take advantage of the power savings of the multiple voltage step architecture while more precisely controlling the total charge delivered to the tissue. Second, if the resistance of electrodes embedded in tissue increases [27] so that the RC product significantly exceeds the maximum desirable stimulation pulsewidth (typically 8 ms in our group's designs), this stepped design will prove less effective. In this case, the electrode voltage profile under constant current stimulation looks more square, and a current source could provide this stimulus from one supply at the minimum required voltage. A network of voltage supplies can be used to drive different electrodes with different impedances or require different threshold charge levels. These circuit solutions may increase device complexity, but the power savings realized can lead to size, safety, and longevity improvements in implanted tissue stimulators, especially those with large numbers of electrodes, such as retinal implants for the blind.

ACKNOWLEDGMENT

The authors would like to thank L. Theogarajan for circuit design help; D. Perreault, R. Sarpeshkar, and M. Markova for their design insights; and J. Rizzo and the VA Center for Innovative Visual Rehabilitation for their support. The Catalyst Foundation provided graduate fellowship support for Dr. Kelly. The authors

would also like to thank the MOSIS Service, and Director C. Pina and W. Hansford, for providing fabrication support at no cost for the Boston Retinal Implant Project.

REFERENCES

- [1] B. Ziaie, M. D. Nardin, A. R. Coghlan, and K. Najafi, "A single-channel implantable microstimulator for functional neuromuscular stimulation," *IEEE Trans. Biomed. Eng.*, vol. 44, no. 10, pp. 909–920, Oct. 1997.
- [2] W. Liu, K. Vichienchom, M. Clements, S. C. DeMarco, C. Hughes, E. McGucken, M. S. Humayun, E. DeJuan, J. D. Weiland, and R. Greenberg, "A neuro-stimulus chip with telemetry unit for retinal prosthetic device," *IEEE J. Solid-State Circuits*, vol. 35, no. 10, pp. 1487–1497, Oct. 2000.
- [3] J. Ohta, T. Tokuda, K. Kagawa, T. Furumiya, A. Uehara, Y. Terasawa, M. Ozawa, T. Fujikado, and Y. Tano, "Silicon LSI-based smart stimulators for retinal prosthesis," *IEEE Eng. Med. Biol. Mag.*, vol. 25, no. 5, pp. 47–59, Sep./Oct. 2006.
- [4] P. R. Troyk, D. E. A. Detlefsen, and G. A. D. DeMichele, "A multifunctional neural electrode stimulation ASIC using neurotalk interface," in *Proc. IEEE 28th Annu. Int. Conf. Eng. Med. Bio. Soc.*, Aug. 2006, pp. 2994–2997.
- [5] L. Theogarajan, J. Wyatt, J. Rizzo, B. Drohan, M. Markova, S. Kelly, G. Swider, M. Raj, D. Shire, M. Gingerich, J. Loewenstein, and B. Yomtov, "Minimally invasive retinal prosthesis," in *Proc. IEEE Int. Solid-State Circuits Conf.*, 2006, pp. 99–108.
- [6] S. K. Kelly and J. L. Wyatt, "A power-efficient voltage-based neural tissue stimulator with energy recovery," in *Proc. IEEE Int. Solid-State Circuits Conf.*, 2004, pp. 228–229.
- [7] K. Gosalia, J. Weiland, M. Humayun, and G. Lazzi, "Thermal evaluation in the human eye and head due to the operation of a retinal prosthesis," *IEEE Trans. Biomed. Eng.*, vol. 51, no. 8, pp. 1469–1477, Aug. 2004.
- [8] A. J. Welch and G. D. Polhamus, "Measurement and prediction of thermal injury in the retina of the Rhesus monkey," *IEEE Trans. Biomed. Eng.*, vol. BME-31, no. 10, pp. 633–644, Oct. 1984.
- [9] *Standard for Safety Levels With Respect to Human Exposure to Radio Frequency Electromagnetic Fields, 3 kHz to 300 GHz*, ANSI and IEEE Std. C95.1-2005.
- [10] R. E. Caulfield, "Power limits influencing retinal prosthesis design," M.S. dissertation, Dept. Elect. Eng. Comput. Sci., Mass. Inst. Technol., Cambridge, MA, 2001.
- [11] S. K. Kelly, "A system for efficient neural stimulation with energy recovery," Dept. Elect. Eng. Comput. Sci., Mass. Inst. Technol., Cambridge, MA, 2004.
- [12] A. G. Dickinson and J. S. Denker, "Adiabatic dynamic logic," in *Proc. IEEE Custom Integrated Circuits Conf.*, May 1994, pp. 282–285.
- [13] W. C. Athas, J. G. Koller, and L. J. Svensson, "An energy-efficient CMOS line driver using adiabatic switching," in *Proc. 4th Great Lakes Symp. VLSI Design Automation of High Performance VLSI Systems*, Mar. 1994, pp. 196–199.
- [14] J. Sit and R. Sarpeshkar, "A cochlear implant processor for encoding music and lowering stimulation power," *IEEE Pervas. Comput.—Special Issue Implant. Electron.*, vol. 1, no. 7, pp. 40–48, 2008.
- [15] J. Sit and R. Sarpeshkar, "A low-power, blocking-capacitor-free, charge-balanced electrode-stimulator chip with less than 6 nA DC error for 1 mA full-scale stimulation," *IEEE Trans. Biomed. Circuits Syst.*, vol. 1, no. 3, pp. 172–183, Sep. 2007.
- [16] X. Beebe and T. L. Rose, "Charge injection limits of activated iridium oxide electrodes with 0.2 ms pulses in bicarbonate buffered saline," *IEEE Trans. Biomed. Eng.*, vol. 35, no. 6, pp. 494–495, Jun. 1988.
- [17] J. F. Rizzo, J. L. Wyatt, J. Loewenstein, S. K. Kelly, and D. B. Shire, "Methods for acute electrical stimulation of retina with microelectrode arrays and measurement of perceptual thresholds in humans," *Invest. Ophthalmol. Vis. Sci.*, vol. 44, no. 12, pp. 5355–5361, 2003.
- [18] J. F. Rizzo, J. L. Wyatt, J. Loewenstein, S. K. Kelly, and D. B. Shire, "Perceptual efficacy of electrical stimulation of human retina with a microelectrode array during acute surgical trials," *Invest. Ophthalmol. Vis. Sci.*, vol. 44, no. 12, pp. 5362–5369, 2003.
- [19] J. D. Weiland and D. J. Anderson, "Chronic neural stimulation with thin-film, iridium oxide electrodes," *IEEE Trans. Biomed. Eng.*, vol. 47, no. 7, pp. 911–918, Jul. 2000.
- [20] S. I. Fried, H. A. Hsueh, and F. S. Werblin, "A method for generating precise temporal patterns of retinal spiking using prosthetic stimulation," *J. Neurophysiol.*, vol. 95, no. 2, pp. 970–978, Feb. 2006.

- [21] R. J. Jensen, O. R. Ziv, and J. F. Rizzo, "Responses of rabbit retinal ganglion cells to electrical stimulation with an epiretinal electrode," *J. Neural Eng.*, vol. 2, no. 1, pp. S16–S21, Mar. 2005.
- [22] H. Pan, Y. C. Liang, and R. Oruganti, "Design of a smart power synchronous rectifier," *IEEE Trans. Power Electron.*, vol. 14, no. 2, pp. 308–315, Mar. 1999.
- [23] H. Jia, X. Cheng, X. Wang, P. Kumar, and Z. J. Shen, "A novel monolithic self-synchronized rectifier," in *Proc. IEEE Applied Power Electronics Conf. Exhibit.*, 2008, pp. 907–912.
- [24] D. B. McCreery, W. F. Agnew, T. G. H. Yuen, and L. Bullara, "Charge density and charge per phase as cofactors in neural injury induced by electrical stimulation," *IEEE Trans. Biomed. Eng.*, vol. 37, no. 10, pp. 996–1001, Oct. 1990.
- [25] A. C. H. MeVay and R. Sarpeshkar, "Predictive comparators with adaptive control," *IEEE Trans. Circuits Syst. II, Analog Digit. Signal Process.*, vol. 50, no. 9, pp. 579–588, Sep. 2003.
- [26] M. Bazes, "Two novel fully complementary self-biased CMOS differential amplifiers," *IEEE J. Solid-State Circuits*, vol. 26, no. 2, pp. 165–168, Feb. 1991.
- [27] S. Cogan, "In vivo and in vitro differences in the charge-injection and electrochemical properties of iridium oxide electrodes," in *Proc. IEEE Int. Conf. Eng. Medicine and Biology Soc.*, 2006, pp. 882–885.



Shawn K. Kelly (M'03) received the B.S., M.Eng. and Ph.D. degrees in electrical engineering from the Massachusetts Institute of Technology (MIT), Cambridge, in 1996, 1998, and 2003, respectively.

He has worked in research positions studying cartilage and brain tissue resistivity at MIT and at the University of Pittsburgh, and as a Test Engineer at M/A-COM. Since 2003, he has been with the Veterans Affairs Center for Innovative Visual Rehabilitation, VA Boston Healthcare System, Boston, MA, as a Research Biomedical Engineer, and as a Visiting

Scientist at MIT. His current research interests include circuit design, power and data telemetry, and power management.

Dr. Kelly is a member of Sigma Xi and the Association for Research in Vision and Ophthalmology.



John L. Wyatt, Jr. (S'75–M'78–SM'95) received the B.S. degree in electrical engineering from the Massachusetts Institute of Technology (MIT), Cambridge, in 1968, the M.S. degree in electrical engineering from Princeton University, Princeton, NJ, in 1970, and the Ph.D. degree in electrical engineering from the University of California, Berkeley, in 1979.

He spent two years in the U.S. Public Health Service developing a cheap sensitive radiation measuring instrument and one postdoctoral year

in the Physiology Department at the Medical College of Virginia, modeling membrane transport phenomena in medicine and biology. He joined the MIT faculty in 1979 and has been a Full Professor in electrical engineering since 1990. He co-directs a joint project with the Harvard Medical School to develop a retinal implant device for the blind. His theoretical interests are in the area of nonlinear and noisy circuits and systems.